THE JOURNAL OF PHYSICAL CHEMISTRY B

Article

pubs.acs.org/JPCB

Access and Binding of H_2S to Hemeproteins: The Case of HbI of *Lucina pectinata*

Fernando M. Boubeta,[†] Sara E. Bari,[†] Dario A. Estrin,[†] and Leonardo Boechi*[,‡]

[†]Departamento de Química Inorgánica, Analítica y Química Física/INQUIMAE-CONICET, Facultad de Ciencias Exactas y Naturales, Universidad de Buenos Aires, Ciudad Universitaria, Pab. II, Buenos Aires C1428EHA, Argentina

[‡]Instituto de Cálculo/CONICET, Facultad de Ciencias Exactas y Naturales, Universidad de Buenos Aires, Ciudad Universitaria, Pab. II, Buenos Aires C1428EHA, Argentina

Supporting Information

ABSTRACT: Hydrogen sulfide (H_2S) was recently discovered as a gasotransmitter, capable of coordinating to the heme iron of hemeproteins. H_2S is unique for its ability to render varying concentrations of the nucleophilic conjugate bases (HS^- or S^{2-}), either as free or bound species with expected outcomes on its further reactivity. There is no direct evidence about which species (H_2S, HS^-, or S^{2-}) coordinates to the iron. We performed computer simulations to address the migration and binding processes of H_2S species to the hemoglobin I of *Lucina pectinata*, which exhibits the highest affinity for the substrate measured to date. We found that H_2S is the most favorable species in the migration from the bulk to the active site, through an internal pathway of the protein. After the coordination of H_2S, an array of clustered water molecules modifies the active site environment, and assists in the subsequent deprotonation of the ligand, forming Fe(III)−SH^-. The feasibility of the second deprotonation of the coordinated ligand is also discussed.

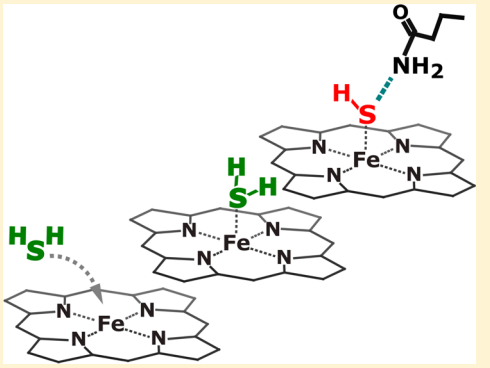

I. INTRODUCTION

The long history of hydrogen sulfide (H_2S) as a deleterious molecule was deconstructed with the discovery that sulfide species are produced and regulated in mammals[1−8] and plants,[9−12] with important biological functions at low concentrations. At the onset of the XXI century, H_2S was included in the family of gasotrasmitters (along with nitrogen oxide and carbon monoxide). In most cases, the function of H_2S is related to reactions with small endogenous thiol compounds,[13,14] protein thiols,[15−17] metalloproteins,[18] and hemeproteins,[19−21] directly impacting the ATP synthesis and the function of potassium channels, with significant outcomes in the muscular tone and neuronal activity in mammals.[22−25] An outstanding example is the reaction of H_2S with the cytochrome c oxidase, where the reversible binding of H_2S decreases the activity of the enzyme,[26,27] inducing hibernation-like states in mice.[28,29] In myoglobin and hemoglobin, diverse forms of reactivity of sulfide have been described: whereas the formation of the so-called sulfheme compounds due to the reaction of sulfide on the heme periphery has been attributed to either deleterious processes[30] or to a detoxification shortcut,[24] the binding of sulfide to the ferric ion of hemoglobin has been recently reported as the initial step of an oxidative, catabolic route for sulfide.[31]

The binding of sulfide to ferric hemeproteins is under active debate both from the chemical and biological standpoints. The affinity constant of Fe(III)−(sulfide)[20,32,33] complexes described to date ranges from ∼10^9 (hemoglobin I of *L. pectinata*, HbI)[32] to ∼10^4 M^{-1} (microperoxidase 11)[34] at physiological pH. For hemeproteins, the affinity has been extensively described in terms of distal stabilization mechanisms, and the reported heme model microperoxidase permitted the dissection of the role of the proximal histidine in aqueous or nonpolar environments.[35] Remarkably, the preferred binding of sulfide to ferric hemes is a feature that distinguishes hydrogen sulfide from siblings carbon monoxide and nitric oxide (both of which bind more strongly to ferrous heme), as is the equilibria with the deprotonated, anionic, and nucleophilic conjugate species, hydrosulfide (HS^-) and sulfide (S^{2-}). It has been speculated that H_2S, and not HS^-, is the bound form to the ferrous/ferric porphyrin of a cytochrome c oxidase model,[27] and the same species was claimed to bind HbI of *L. pectinata*.[33] Conversely, it was assumed that HS^- is the main species that binds to *T. fusca* hemoglobin.[36] The identification of the coordinated sulfide species (H_2S, HS^-, or S^{2-}) should be under cautious scrutiny because it is crucial for the resulting affinity and the subsequent reactivity.

As the pK_{a1} of H_2S is ∼7.0, the neutral form coexists with the hydrosulfide monoanion (HS^-) under physiological conditions. The pK_a of the coordinated H_2S may differ from that found in the bulk solvent due to both the electronic character of the Fe−S bond and the role of the surrounding

Received: July 4, 2016
Revised: July 27, 2016

DOI: 10.1021/acs.jpcb.6b06686
J. Phys. Chem. B XXXX, XXX, XXX−XXX

environment (e.g., solvent molecules, distal amino acids, etc.). Moreover, the coordinated species may indeed be different from the one that migrates from the bulk to the heme cavity, as migration and binding may be considered as independent events.

Computational chemistry on hemeproteins has been widely used[33,37−43] and proved to be a good strategy to describe molecular details concerning hemic systems and as a prediction tool of relevant biological processes.

In order to elucidate the molecular details underlying the binding and reactivity of sulfide species to hemeproteins, we performed a variety of computer simulations considering the case of HbI from *L. pectinata*.

II. THEORETICAL METHODS

Preparation of the Systems and MD Simulation Parameters. The protein structures of 5c, Fe(III)−SH_2, and Fe(III)−SH^- states were constructed from the X-ray structure file corresponding to PDB id 1b0b (HbI of *L. pectinata*), to which the corresponding ligand coordinated to the iron center (H_2S and HS^-) was added. The fixed protonation states amino-acids protonation were assumed to correspond to physiological pH (i.e., Asp and Glu negatively charged, Lys and Arg positively charged), all solvent exposed His were protonated at the N-δ delta atom, as well as the proximal His, which is coordinated to the iron heme. Crystallographic water molecules were deleted manually, and the system was solvated by constructing an octahedral box of 10 Å. Approximately 6840 TIP3P water molecules were placed inside the box through the standard criteria procedure of the AmberTools Package.[44] Parameters of all residues (except for the heme group) were taken from the AMBER ff99SB force field.[45]

To obtain representative AMBER parameters for the MD simulations, a model system consisting of an imidazole ring ligand bound through its N-δ to a ferric iron-porphyrin complex without lateral groups (vynils, methyls, or propionates) was used to represent the heme group of the protein. Finally, in the trans position of the imidazole ring, H_2S or HS^- ligand was coordinated to the iron.

Full QM geometry optimization was performed for the three complexes under DFT approximation using the Gaussian 03 program.[46] DFT calculations have been extensively applied to metalloproteins in general and to iron-porphyrin systems in particular.[47−52] The DFT calculations reported in this Article employed PBE as both the correlation and exchange functional developed by Perdew, Burke, and Ernzerhof in 1996[53] and 6-31G** as basis sets. In each optimization procedure, frequency calculations using normal mode approximation were performed to check that a local minimum in the potential energy surface was obtained. In this work, the total charge and electronic spin of 5c, H_2S, and HS^- systems have been imposed to set ferric low spin (S = 1/2) for the 6th coordinated complexes and ferric high spin (S = 5/2) for the 5c complex (full QM optimized coordinates of 5c and 6th coordinated structures, including the total energy, are available in the Supporting Information as .pdb files).

Bonds, angles, and torsional parameters including Fe atom and sulfide species were obtained from the full QM-optimized structures by scanning the potential energy surface around the minimum of the coordinate of interest. The resulting energy profiles were fit to the appropriate AMBER potential functional form. We used the parameters previously obtained in our group for the rest of the porphyrin system.[50,54] Partial atomic charges were obtained using the restrained electrostatic potential (RESP) procedure for the optimized systems, from single-point PBE/6-31G** calculations and the CHELPG[55] based method and imposing symmetry on equivalent atom types.

The procedure described above was validated and widely used in several studies of hemeproteins from our group.[56−58]

All MD simulations were performed using periodic boundary conditions with a 9 Å cutoff and the particle mesh Ewald (PME) summation method for treating the electrostatic interactions. The covalent bonds involving hydrogen atoms were restrained at their equilibrium distance by using the SHAKE algorithm, while the temperature and pressure where kept constant with a Berendsen thermostat and barostat, respectively, as implemented in the AMBER14 package.[44]

For the three structures (5c, Fe(III)−SH_2, and Fe(III)−SH^-), the equilibration protocol consisted of (i) slowly heating the whole system from 0 to 300 K for 2 ns at constant volume, with harmonic restraints of 80 kcal/mol·Å^2 for all Cα atoms and (ii) slowly heating from 0 to 300 K for 2 ns at constant preasure of the entire system. (iii) After these two steps, an unconstrained ∼300 ns molecular dynamics simulation at constant temperature (300 K) and pressure was performed, in order to obtain systems described by the NPT ensemble.

For the sake of convergence, we used two strategies: (a) on each state, starting from the same initial structure described above, three different equilibration protocols were applied by varying the equilibration parameters (total simulation time, restraints, etc.). This procedure leads to three uncorrelated replicas of each state, obtaining a total simulation time of 600 ns for each state. (b) Taking three different uncorrelated structures from the first MD trajectory and restarting the velocities, we extended the MD trajectories for 300 ns for each state.

All together, we obtained approximately 1.3 μs of MD trajectories for each state. All structures were found to be stable during the time scale of simulations, as evidenced by the root mean square deviation analysis shown in the Supporting Information (Figure S1).

Implicit Ligand Migration (ILS) Calculation. ILS evaluates the free energy cost of placing a small ligand at any desired positions in the system of interest taking into account different orientations. The regions that are accessible to the ligand are characterized by low free energy values. Thus, if those regions are connected by sufficient low free energy regions, an internal pathway (IP) can be defined. It is important to remark that this technique allows a simultaneous determination of several different IPs of a protein in a completely unbiased way.

In order to have representative results using trajectories performed in the absence of the ligand, this approach assumes that the ligand interacts weakly with the protein matrix.[59,60]

ILS has been shown to be a good strategy for prediction of IPs for small neutral ligands in hemeproteins.[61−64]

Technically, the method uses MD simulations of the system without explicitly considering the ligand of interest, and evaluates the free energy (through the probability) of finding the ligand at several positions (and orientations) using a grid. The probability is evaluated in the presence of the "implicit" ligand, considering it as a small perturbation in the

DOI: 10.1021/acs.jpcb.6b06686
J. Phys. Chem. B XXXX, XXX, XXX−XXX

Hamiltonian of the original system, described as a term of interaction between ligand and protein.

In this work, ILS calculations were performed in a regularly spaced rectangular grid of 0.5 Å resolution that includes the protein, the probe used was a H_2S molecule, and five different orientations were taken into account.

The interaction was considered as a Lennard-Jones term, truncated at 9 Å, probe parameters used for the interactions belong to the AMBER force field, and the geometric parameters were taken from full-QM geometry optimization for the probe (at the PBE/6-31G** level).

It is important to remark that, because HS^- is a charged ligand, the ILS methodology is inappropriate. This is due to computational expense of long-range Coulombic interactions for several positions and orientation of the ligand. In addition, the requirement of small interaction between protein and ligand could not be satisfied, possibly generating conformational changes that could not be evaluated in the trajectories used as reference.[60]

Calculations were performed on 4000 frames taken from 1200 ns of simulation time of the 5c state of the protein. Finally, an IP was considered as a zone connecting the active site with the solvent within values of free energy less than 1.5 kcal/mol.

To check the convergence, we divided the total number of frames into three blocks of 1000 frames, and we analyzed them separately. Similar results were obtained for the three blocks, as evidenced in the Supporting Information (Figure S2). All ILS calculations were performed using the VMD 1.9.1 module program.[65]

Steered Molecular Dynamics (SMD). SMD is an efficient way to explore the system along a defined reaction coordinate,[66,67] usually modifying the original description of the system by adding a harmonic guiding potential over a selected arbitrary reaction coordinate (ξ). This potential is characterized by a spring constant, and a center of the spring. In order to cover the relevant region of the reaction coordinate, the center of the spring is linearly modified based on an arbitrary velocity (v).

Employing this modified system and starting from N different initial microconfigurations well described by a convenient thermodynamic ensemble (NPT in our case, see below), it is possible to calculate the accumulated work for several independent nonequilibrium change processes, $w_i(\xi, v)$, by sampling the reaction coordinate chosen from an initial to a final value, according to the guiding potential and velocity v. With these data, it is possible to employ the Jarzynski equality[68] (JE, eq 1) to obtain the free energy profile of the process along the reaction coordinate sampled

$$e^{[-\beta\Delta G(\xi)]} = \langle e^{[-\beta W_i(\xi,v)]}\rangle_N \quad (1)$$

where $\beta = (k_B \cdot T)^{-1}$, k_B is the Boltzmann constant, and T is the absolute temperature, and the average is performed over a set of N pulling trajectories. In principle, this relation holds for any velocity selected for the sampling and for a sufficient amount of data evaluated. In this case, ΔG will converge to the free energy difference associated with the initial and final reaction coordinate sampled. The error analysis of the free energy profiles is a crucial issue. A detailed description of the error analysis is given in the Supporting Information.

We evaluated the free energy profile of H_2S and HS^- along the internal pathway of *L. pectinata* choosing the Fe−S distance as the reaction coordinate.

JE requires that the modified system must be well equilibrated under the desired ensemble to work (we select the NPT ensemble), with the restraint fixed at the initial value of the reaction coordinate. Therefore, we selected a snapshot from the MD simulation of the 5c state of the protein and we placed H_2S (or HS^-) at ∼9 Å for the distance between Fe and S atoms, the chosen position was that we regard as the entrance of the IP found by ILS calculation.

Initial restrained MD (5 × 100 ns with H_2S and HS^-, respectively) simulations were performed with position fixed at that initial value of the reaction coordinate (∼9 Å) using a value of 200 kcal/(mol·Å) for the spring constant, and using the same parameters for the MD described in the MD section. Saving different snapshots every 1 ns of the run, we obtained 500 uncorrelated initial snapshots with fixed reaction coordinate to ∼9 Å. Snapshots in which the ligand is far from the entrance of the IP were discarded; the rest of them were used to perform the change process varying the reaction coordinate from 9 to 4 Å using a spring constant of 200 kcal/(mol·Å^2) and using a pulling velocity of 0.0025 Å/ps. The spring constant and pulling velocity for the SMD simulations were chosen following the computational scheme reported in previous studies.[64,69,70] In this case, the pulling velocities were chosen to be 10 times slower than in previous works, in order to improve the convergence.

Finally, perturbations in which the ligands migrated beneath the heme ring were also discarded, as they do not represent the process of interest.

At the end of the procedure described above, a set of 378 work profiles for H_2S and 193 for HS^- were obtained for the analysis. The JE was then evaluated at each value of the reaction coordinates, and the free energy profiles were constructed.

Characterization of Water Sites (WS). Water sites correspond to specific regions inside the protein that can host a water molecule with a probability value higher than a water molecule surrounded by the bulk environment. In our previous works, we show that these regions can be identified by computing the probability of finding a water molecule inside a defined region during MD simulation performed with explicit solvent water molecules.[71−73]

The region volume used to identify WS was arbitrarily set to 1 Å^3, and the WS center coordinates correspond to the average position of all the water oxygen atoms that visit the WS along the simulation. A water molecule is considered as occupying that WS when the distance between the position of its oxygen atom and the WS center value is less than 0.6 Å.

Once identified, for all potential WS, we computed the water finding probability (WFP), corresponding to the probability of finding a water molecule in the region defined by the WS and normalized with respect to the bulk solvent probability to harboring a water molecule in a sphere of the same volume at the corresponding temperature and pressure values; thus, the WFP is actually used as a cutoff value to decide which potential WS are relevant. In this work, only WS with WFP values greater than 2 are retained.

All WS calculations were performed using the VMD module named WATCLUST program,[74] with default parameters and considering that a WS is formed when the water molecules were hosted more than 10% of the time scale

DOI: 10.1021/acs.jpcb.6b06686
J. Phys. Chem. B XXXX, XXX, XXX−XXX

of the MD simulation analyzed. We used ~3000 frames of the whole MD simulations on each state to determine WS (same amount of frames for the 50 ns MD simulation "switching" procedure described in the Results section). Convergence was also checked using different segments of all the MD simulations used to define WS, ensuring that the WS definition was robust (data not shown).

Sulfide QM/MM Energy. QM/MM calculations were performed for H_2S or HS^- coordinated to the Fe(III) atom of HbI of *L. pectinata*. The initial structures for the QM/MM calculations were obtained from the corresponding previously described MD simulations. Selected snapshots based on the structure and dynamics analysis of the hydrogen bond pattern for each case were selected and cooled down slowly to 0 K. Starting from these frozen structures full hybrid QM/MM geometry optimizations were performed using a conjugate gradient algorithm, at the DFT level with the numerical basis set SIESTA code using our own QM/MM implementation called Hybrid.[75] For all QM atoms, basis sets of double beta plus polarization quality were employed. All calculations were performed using the generalized gradient approximation functional proposed by Perdew et. al[54] (named PBE) for both exchange and correlation functional. This correlation-exchange functional has been used in several works in order to describe the reactivity of small molecules in hemeproteins.[57,76] In addition, it also has been proved to be reliable for describing reactions that include proton transfer processes.[77−79]

For all systems studied, the spin unrestricted approximation was used, and we use the term "low spin" as a doublet state and "high spin" as a sextet state. Only residues located less than 10 Å apart from the heme reactive center were allowed to move freely in the QM/MM procedures. The QM subsystem included the heme group (without the peripheral groups), the H_2S or HS^- ligands, as the case Gln (or Ala), and the imidazole ring of the proximal side. The rest of the protein unit, together with water molecules, was treated classically. The interface between the QM and MM portions of the system was treated by the scaled position link atom method. This strategy has been widely and successfully used in our group mainly in biomolecules.[57,80−86]

Since obtaining accurate free energy profiles requires extensive sampling, which is computationally very expensive and difficult to achieve at the DFT QM/MM level, we resorted to computing potential energy profiles using restrained energy minimizations along the reaction coordinate that describe the deprotonation process. For this approach, an additional term, $V(\xi) = k[\xi - \xi_0]^2$, is added to the potential energy, where k is an adjustable force constant (set to be 200 kcal/mol·Å^2) and ξ_0 is a reference value, which is varied stepwise along the reaction coordinate with an interval of 0.5 Å along the reaction coordinate. By varying ξ_0, the system is forced to follow the energy minimum reaction path along the given reaction coordinate ξ.

Sulfide QM/MM-MD Simulations. QM/MM-MD simulations were carried out using the Gaussian basis set DFT Lio module implemented in the Amber package.[87,88] Force field parameters and the protocol for the thermalization step can be found elsewhere.[89] In the present work, the QM and MM partioning of the system was similar to that used for the QM/MM optimizations described in the previous section. The difference in the QM portion (as we obtain similar results using several or one water molecule) is that we decided to include only one water molecule. We employed the scaled position link atom to describe the QM/MM boundaries.[75] For the QM region, computations were performed at the generalized gradient approximation (GGA) level, using the PBE combination of exchange and correlation functionals, with a dzvp basis set for the expansion of the one electron orbitals in a spin unrestricted approximation using charge and spin state to obtain the Fe(III)−SH_2 complex at low spin state; in this case, we assume spin multiplicity of 2 units. The electronic densities were also expanded in an auxiliary basis set, and the coefficients for the fitting were computed by minimizing the error in the Coulomb repulsion energy.

Initial configurations were generated from the MD classical simulations of the Fe(III)−SH_2 state in which the solute was treated classically as a rigid moiety, followed by a 100 ps MM simulated annealing from 300 to 0 K, and QM/MM energy optimization procedure. Finally, a thermalization procedure was performed from 0 to 300 K using the Langevin dynamic scheme. We employed the Verlet algorithm to integrate Newton's equations with a time step of 1 fs. Temperature was held constant at 300 K using the Langevin thermostat. All

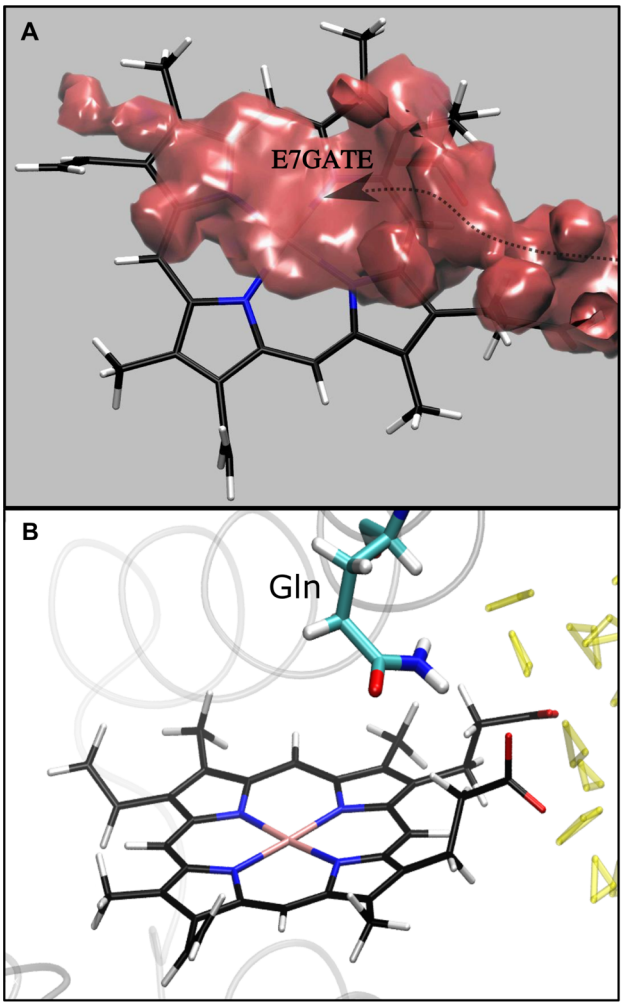

Figure 1. (A) Free energy isosurface (1.5 kcal/mol isovalue) computed with implicit ligand sampling of H_2S in hemoglobin I of *L. pectinata*, in the 5c ferric state. (B) Detail of the E7 gate IP, where solvated heme propionates and polar Gln residue are depicted. Atoms in red and blue are representing charged groups, and water molecules are depicted in yellow.

DOI: 10.1021/acs.jpcb.6b06686
J. Phys. Chem. B XXXX, XXX, XXX−XXX

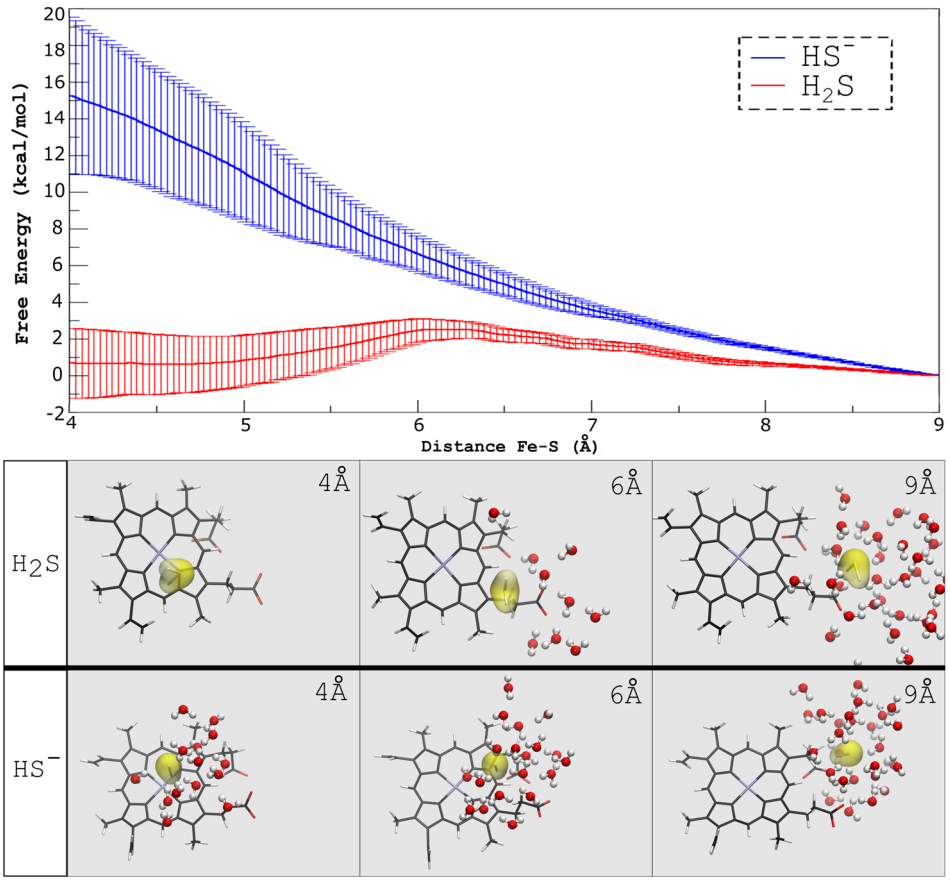

Figure 2. Upper panel: Free energy profile of H_2S (red) and HS^- (blue) migration through the E7 gate internal pathway of HbI. RMSE values are depicted as error bars on each profile. Lower panels: Representative snapshots taken from the SMD trajectories for H_2S and HS^- at different Fe−S distances (from left to right 4, 6, and 9 Å, respectively). In all cases, water molecules located at less than 5 Å of the sulfur atom are depicted.

dynamics and statics calculations were visualized with VMD 1.9.1.[65]

III. RESULTS

Characterization of Internal Pathways. An internal pathway (IP) is the area drilled inside the protein matrix that connects zones of low free energy (known as "transient cavities") that can be formed by thermal fluctuations of a protein structure. It is well-known that some proteins of the globin family present various IPs connecting, ultimately, the active site with the solvent. The IP and the water molecules in the active site have been proposed to play a key role in determining ligand migration through the protein matrix and binding to the metal center.[90−93]

We performed implicit ligand sampling (ILS) calculations of the protein in the ferric penta coordinated (5c) state of the iron. We used H_2S as the probe molecule. We note that the ILS method cannot be used to evaluate differences between H_2S and HS^-, as the probe only provides qualitative evidence about potential pathways for small ligands.

We found one IP that connects the solvent with the active site (Figure 1A). This pathway corresponds to the so-called "E7 gate" found in both myoglobin and hemoglobin.[94,95] Figure 1B zooms in on the vicinity of the IP, depicting the solvated propionate side chains and a distal Gln residue.

Free Energy Profile of Migration of the Sulfide Species (H_2S vs HS^-). In order to evaluate the differences between H_2S and HS^- ligands, we calculated the ligand migration free energy profile along the E7 pathway, by performing steered molecular dynamics (SMD) simulations combined with the Jarzynski equality (Figure 2). The Fe−S distance was chosen as the reaction coordinate. The combination of SMD and the Jarzynski equality has been successfully applied to several studies in proteins.[64,70,96−98]

Our results show that H_2S is the most favorable species to migrate to the active site (Figure 2, upper panel), with a low barrier (∼2 kcal/mol) and a low free energy difference between the bulk solvent and the active site of ∼1 kcal/mol. On the other hand, HS^- displays a very high barrier and a free energy difference between the bulk solvent and the active site of approximately 16 kcal/mol, with no apparent free energy minimum as the ligand reaches the active site (at approximately 4 Å). The profiles are ended at 4 Å from the iron atom, as the classical force field used is not able to describe the electronic interaction during Fe−S bond formation.

Details about the convergence criteria used in our SMD calculations are included in the Supporting Information (Figure S3).

The difference between the two free energy profiles can be rationalized by inspecting the individual SMD trajectories for both ligands. When H_2S migrates from the bulk to the active site, its solvation structure changes dramatically, expelling water molecules from its surroundings as it reaches the active site (Figure 2, lower panels). On the contrary, HS^- migrates

DOI: 10.1021/acs.jpcb.6b06686
J. Phys. Chem. B XXXX, XXX, XXX−XXX

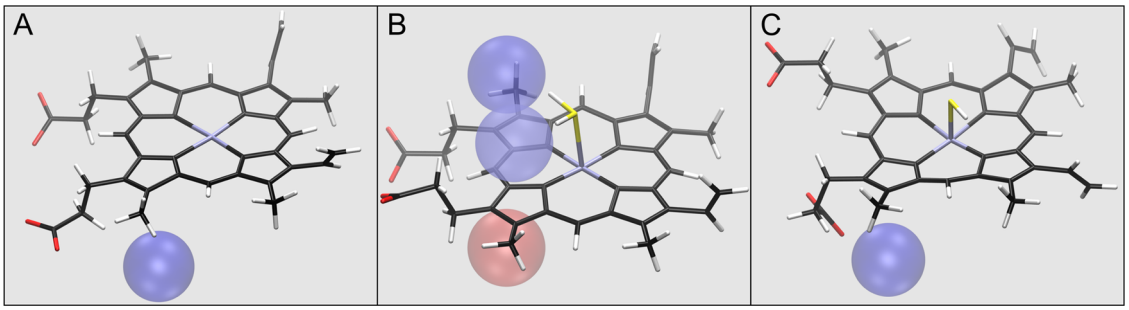

Figure 3. WS observed in the 5c (A), 6c H_2S (B), and 6c HS^- (C) ferric states HbI of *L. pectinata*. Red and blue regions represent the low and high probability of finding a water molecule with respect to the solvent, respectively. The three cases present WS in the proximal site of the heme group (below the heme in the figure), which is not involved in sulfide binding. The proximal histidine ligand has been omitted for clarity.

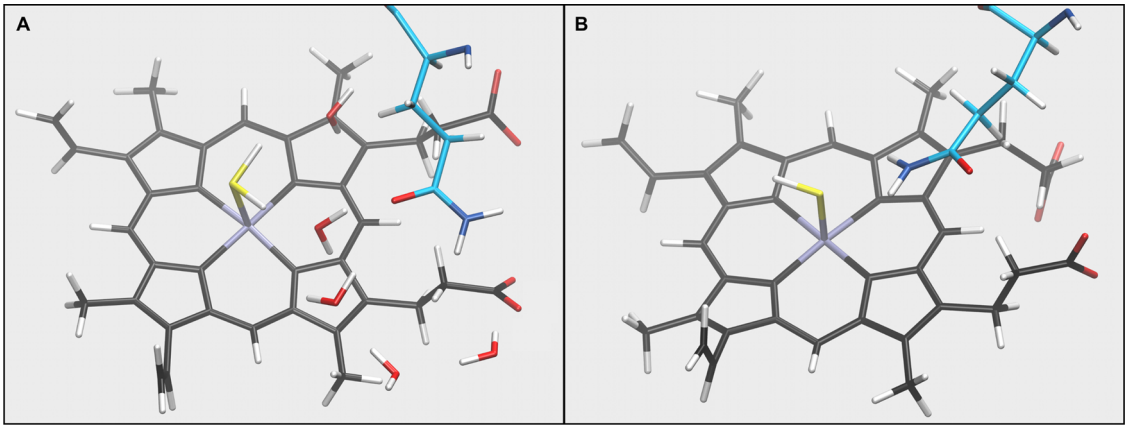

Figure 4. Stabilization of the coordinated H_2S and HS^- during MD simulations. (A) Representative snapshot of the hydrogen bond interaction between Gln and H_2S in the Fe(III)−SH_2 complex; water molecules around Gln65 are also depicted showing the interaction between coordinated H_2S and Gln residue. (B) Representative snapshot of the hydrogen bond interaction between the N(Gln) and S atom in the Fe(III)−SH^- complex.

to the active site still solvated, most likely due to its net charge.

Formation of Water Sites in the Active Site. It was observed that water molecules, strongly stabilized in the active site, can slow down the ligand binding process, mainly because a water displacement process must occur in advance.[90−92] A water site (WS) is defined as a spatial region in a system with a high probability of finding water molecules, as compared with the probability of finding water molecules in the bulk solvent. Each WS is characterized by a water finding probability (WFP). The position of each WS is defined by the coordinates of the maximum probability point within a selected region. We performed WS calculations using MD trajectories for the 5c, Fe(III)−SH_2, and Fe(III)−SH^- states, considering a WS as the zone where water molecules are present in at least 10% of the time scale of the trajectory analyzed.

Distal WS were not observed prior to the addition of sulfide, as depicted in Figure 3A. We found, however, two distal WS in the Fe(III)−SH_2 state (Figure 3B). In this case, the carbonyl group of Gln65 interacts with the S atom of the coordinated H_2S via a bridging water molecule. In the case of HS^-, no distal WS was observed (Figure 3C). We note that in all three cases a WS was identified in the proximal side of the heme group. Although this particular WS is conserved, it does not participate in the Fe−S bond formation.

We provide further evidence about the convergence of WS calculation in the Supporting Information (Figure S4).

The absence of a WS in the Fe(III)−SH^- state evidences a decrease in the polarity of the active site, as compared to the Fe(III)−SH_2 state (Figure 3C). We note that the conformations of distal site residues Phe30, Phe44, and Phe69 do not undergo significant changes in going from the 5c to the Fe(III)−SH_2 and Fe(III)−SH^- states.

A close inspection of the distal site reveals that the amino N atom of Gln65 is able to form a hydrogen bond with the S atom in the Fe(III)−SH^- complex, avoiding WS formation (Figure 4B). In the Fe(III)−SH_2 complex, however, Gln65 assists the formation of two WS in the vicinity of the active site, which interact with the coordinated H_2S (Figure 4A).

First Deprotonation Step: from Fe(III)−SH_2 to Fe(III)−SH^-. In the previous section, we showed that H_2S and not HS^- is the species that preferentially migrates through the polar E7 gate IP of Hb I of *L. pectinata*. In this section, we show the results of QM/MM calculations for the eventual deprotonation of the coordinated H_2S.

We found that the deprotonation process of the bound H_2S is thermodynamically favorable (negative ΔE values for the global process) and that the process occurs with no barrier (Figure 5A). We also observed that the proton is transferred from the Fe(III)−SH_2 to one of the water molecules in the observed WS, and subsequently to the carbonyl group of the Gln65 (Figure 5B and C). No significant differences were found for the high and low spin states (Figure 5A).

As a control experiment, we performed QM/MM calculations with Fe(III)−OH_2 instead of Fe(III)−SH_2. In

DOI: 10.1021/acs.jpcb.6b06686
J. Phys. Chem. B XXXX, XXX, XXX−XXX

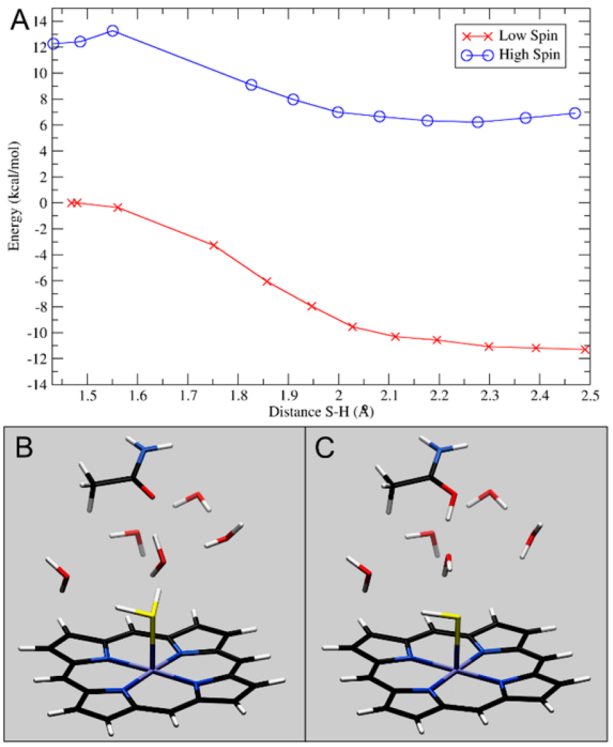

Figure 5. Fe(III)−SH_2 deprotonation energy profile HbI of *L. pectinata* (A); red and blue profiles correspond to low and high spin states, respectively. (B and C) Initial and final snapshots of the energy profile are also shown. The reaction coordinate was the S−H distance.

this case, the global ΔE value was positive, meaning that a water molecule is less prone to release a proton (Figure S5). Similar results were obtained using either only one water molecule (belonging to the "bridge-like" WS) or two (one in each WS) water molecules in the QM subsystem for both Fe(III)−SH_2 and Fe(III)−OH_2 (data not shown). To evaluate the relevance of Gln65 in the deprotonation process, we performed the same calculations for the Gln65Ala mutant (Figure 6).

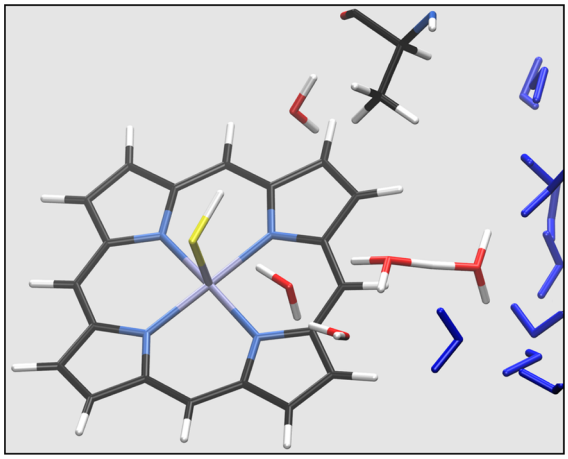

Figure 6. QM/MM optimized structure for the Fe(III)−SH_2 complex in HbI of *L. pectinata*, mutating Gln to Ala in a ferric low spin state. Several MM water molecules belonging to the bulk are depicted in blue (the QM imidazole ring of histidine was omitted for clarity). Similar results were obtained for the high spin state.

In both low and high spin states, the deprotonation occurs during the optimization step of the calculation. This result evidences that Gln65 is not required for the deprotonation but that it may assist in making the process more favorable.

In order to add more evidence about the deprotonation of the coordinated H_2S and the role of the Gln65 in the process, we performed QM/MM-MD simulations. This methodology allows us to sample more configurational space than traditional QM/MM optimizations (see Methods for details). In the thermalization step of the calculation, the proton is spontaneously transferred from the Fe(III)−SH_2 to the water molecule in the WS and then toward the Gln65 (Figure 7),

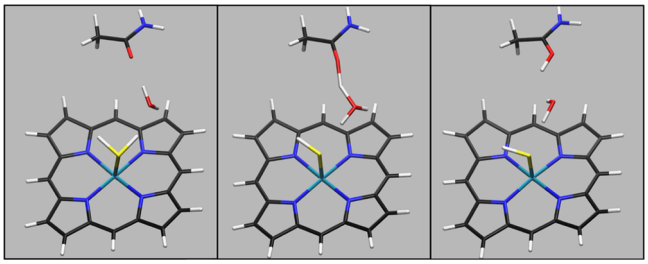

Figure 7. Subsequent snapshots for the Fe(III)−SH_2 deprotonation process in the thermalization step of the QM/MM-MD for the QM portion of HbI of L. *pectinata* in HbI of *L. pectinata*. The QM imidazole ring of histidine was omitted for clarity.

evidencing that the deprotonation process is thermodynamically favorable at room temperature, consistent with the results from the QM/MM optimizations. A video of the trajectory of the QM portion of the system for the thermalization step is provided in the Supporting Information.

Second Deprotonation Step: from Fe(III)−SH^- to Fe(III)−S^{2-}. We evaluated the feasibility of the second deprotonation of H_2S (to S^{2-}) by performing QM/MM calculations for the Fe(III)−SH^- adduct. Considering that the kinetic barrier for the deprotonation would be very high because of the absence of water molecules in the MD simulation of the Fe(III)−SH^- state (Figure 3C), we instead decided to evaluate the posibility of a fast second deprotonation before the WS exhibited in the Fe(III)−SH_2 adduct are dissassembled. For this purpose, we started the simulation with the same structure used for Fe(III)−SH_2. As for the Fe(III)−SH_2 system, deprotonation of Fe(III)−SH^- was favorable under the described conditions (Figure 8). In the onset of the restrained optimization, one proton was

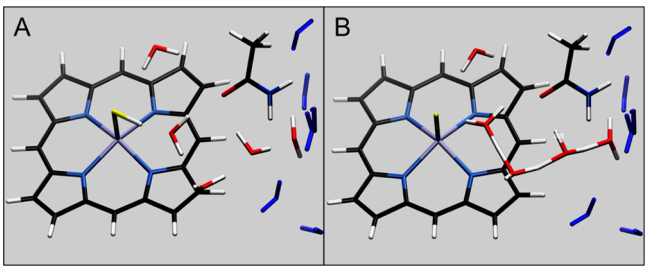

Figure 8. Deprotonation of Fe(III)−SH^- in HbI of *L. pectinata* in a ferric low spin state. Panel A shows the initial structure used for the optimization. Panel B shows the final structure obtained after the QM/MM optimization. Several classical water molecules belonging to the bulk are depicted in blue (the QM imidazole ring of histidine is not depicted). Similar results were obtained for the high spin state.

DOI: 10.1021/acs.jpcb.6b06686
J. Phys. Chem. B XXXX, XXX, XXX−XXX

Scheme 1. Proposed Mechanism for Sulfide Speciation in HbI of *L. pectinata*

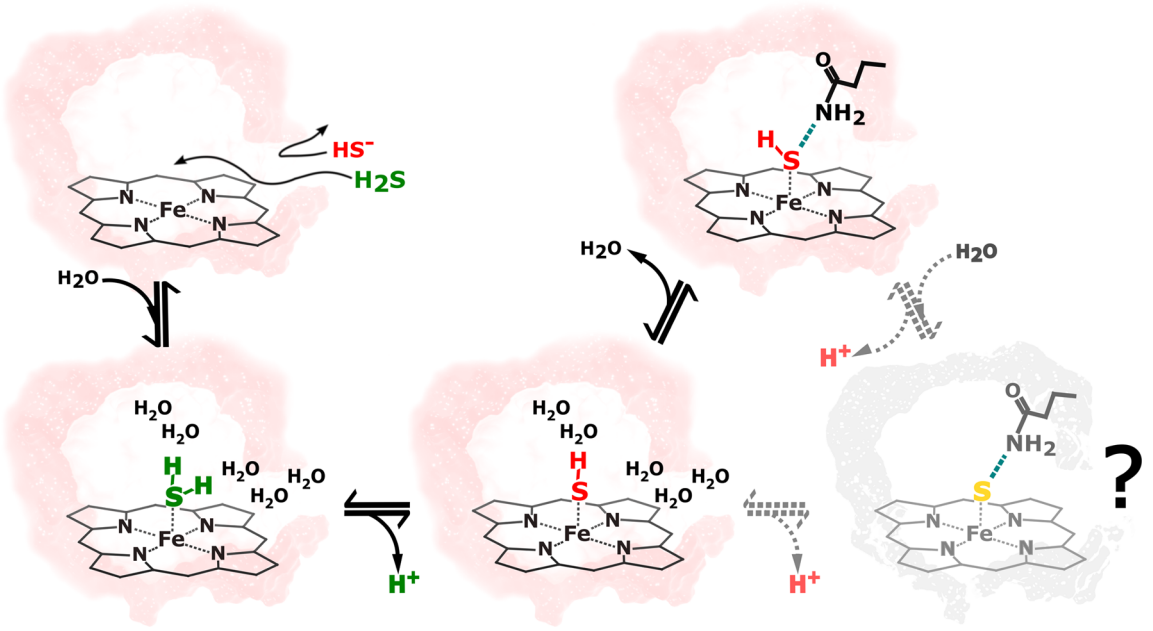

delocalized in the chain of water molecules. This process has a slightly negative global ΔE value with almost no barrier for the proton transfer from the coordinated HS^- to the last water molecule (−4 and 0.1 kcal/mol for low and high spin states, respectively). Under these conditions, the deprotonation process occurs without intervention of Gln65, leaving a delocalized proton among the water molecules connected to the solvent. Considering the small value of ΔE, we cannot provide conclusive evidence about the second deprotonation step, since this result may be dependent on the details of the model.

IV. DISCUSSION

From the results of the ILS, SMD, and QM/MM calculations obtained in this work, we provide new information about the impact of the ionic equilibria of H_2S on its migration and binding to the Fe(III) of HbI of *L. pectinata*.

An internal pathway, which corresponds to the well studied E7 gate of hemoglobin, was found in HbI of *L. pectinata*. Free energy profiles for ligand migration through this IP show that the overall difference in Gibbs free energy (ΔG) along the sampled selected coordinate is larger for HS^- than for H_2S. This difference can be attributed to the higher polarity of HS^-, as the active site is largely hydrophobic. There is a balance between the desolvation of HS^- and the cost of HS^- entering still solvated by many water molecules. Both scenarios generate high free energy barriers for HS^- migration.

The small barrier obtained for H_2S corresponds to the desolvation process that takes places up until approximately 6 Å. Beyond that coordinate value, the free energy profile goes downhill due to the stabilization of the ligand in the hydrophobic environment.

It is interesting to note that, although H_2S migrates mainly devoid of surrounding water molecules, WS are formed after coordination, and on the other hand, HS^- migrates surrounded by water molecules and WS are not formed after coordination. The only way to reconcile this apparent discrepancy in solvation is to conclude that the migrating species is indeed H_2S, and the formation of the Fe(III)−SH^- adduct is the result of the subsequent deprotonation of the coordinated H_2S ligand.

The different behavior between coordinated ligands may be explained from the charge distribution of the sulfide ligands after coordination. H_2S charge becomes more positive when it coordinates, which attracts water molecules and the carbonyl group of Gln. However, for HS^-, when it coordinates, its negative charge density keeps a significant negative charge that attracts the amino moiety of the Gln that hampers the WS formation.

We can enrich the analysis by considering the pK_{a1} values of H_2O and H_2S, ∼14 and ∼7, respectively. It has been demonstrated that, upon coordination to a Fe(III), the pK_{a1} value for coordinated H_2O in hemeproteins decreases at least 4 and as much as 7 pK_a units.[32,99−103] Thus, if we assume that the behavior in the pK_a values is similar for H_2S, the equilibrium that should be taken into account for sulfide species in biorelevant neutral environments should be Fe(III)−SH^-/Fe(III)−S^{2-}. Our QM/MM results show that the first deprotonation step of the Fe(III)−SH_2 complex is thermodynamically favorable. A negative global ΔE (about −10 kcal/mol) and spontaneous proton transfer process in our QM/MM-MD was observed for the Fe(III)−SH_2 complex. Due to the presence of water molecules in the active site, no appreciable kinetic barrier for the proton transfer exists. The results for Fe(III)−SH^- deprotonation show, however, a less negative global ΔE (approximately −2 kcal/mol). Considering the small magnitude of this value, we cannot conclude if the deprotonation of Fe(III)−SH^- occurs spontaneously or not.

On the basis of our classical and QM-MM simulations, we propose the following mechanism (Scheme 1) for the global binding process of sulfide species in HbI of *L. pectinata*: H_2S migrates from the solvent to the active site and coordinates the iron. Immediately afterward, two water sites are formed in the active site bridging the coordinated ligand with Gln65. One of the WS accepts a proton from the coordinated H_2S

DOI: 10.1021/acs.jpcb.6b06686
J. Phys. Chem. B XXXX, XXX, XXX−XXX

and transfers it either to Gln65 or to another water molecule oriented toward the bulk. This process leads to the formation of the Fe(III)−SH^- complex, which subsequently either quickly releases the second proton to a water molecule resulting in the Fe(III)−S^{2-} state or remains in the Fe(III)−SH^- stabilized by Gln65.

Our results show clearly that Fe(III)−SH_2 is not the thermodynamically nor the kinetically stable species. Instead, Fe(III)−SH^- emerges as the bound species, although we cannot conclusively disregard the formation of Fe(III)−S^{2-}.

■ ASSOCIATED CONTENT

Supporting Information

The Supporting Information is available free of charge on the ACS Publications website at DOI: 10.1021/acs.jpcb.6b06686.

Trajectory of the QM portion of the QM/MM-MD thermalization step of the Fe(III)−SH_2 state of HbI of L. *pectinata* (MPG)

Full QM-optimized coordinates of 5c (high spin) complex, including the QM energy (PDB)

Full QM-optimized coordinates of Fe(III)−SH_2 (low spin) complex, including the QM energy (PDB)

Full QM-optimized coordinates of Fe(III)−SH^- (low spin) complex, including the QM energy (PDB)

Figure S1, root mean square deviation for the MD trajectories of 5c, Fe(III)−SH_2 and Fe(III)−SH^- states of HbI of L. *pectinata*; Figure S2, ILS analysis for three blocks of 1000 frames of the whole MD trajectory of the 5c state from HbI of L. *pectinata*; Figure S3, error analysis (RMSE) and details about the convergence criteria for the SMD calculation; Figure S4, evidence about the convergence of WS calculation for the Fe(III)−SH_2 and Fe(III)−SH^- states of HbI of L. *pectinata*; Figure S5, QM/MM energy profile for the restrained optimization for the Fe(III)−OH_2 complex from HbI of L. *pectinata* (PDF)

■ AUTHOR INFORMATION

Corresponding Author

*E-mail: lboechi@ic.fcen.uba.ar. Phone: +005411-45763380, ext. 123.

Notes

The authors declare no competing financial interest.

■ ACKNOWLEDGMENTS

We thank Mehrnoosh Arrar for closely reading and editing the manuscript. F.M.B. thanks the Agencia Nacional de Promoción Científica y Tecnológica (ANPCyT) and Consejo Nacional de Investigaciones Científicas y Técnicas (CONICET) for a doctoral fellowship. D.A.E., L.B., and S.E.B. are CONICET staff. L.B. is the recipient of a Pew L.A. Fellowship. We thank the University of Buenos Aires, ANPCyT (PICT-BID2014-1022), and CONICET for financial support. PICT-BID2014-1022.

■ REFERENCES

(1) Warenycia, M. W.; Goodwin, L. R.; Benishin, C. G.; Reiffenstein, R. J.; Francom, D. M.; Taylor, J. D.; Dieken, F. P. Acute Hydrogen Sulfide Poisoning. Demonstration of Selective Uptake of Sulfide by the Brainstem by Measurement of Brain Sulfide Levels. *Biochem. Pharmacol.* **1989**, *38* (6), 973−981.

(2) Goodwin, L. R.; Francom, D.; Dieken, F. P.; Taylor, J. D.; Warenycia, M. W.; Reiffenstein, R. J.; Dowling, G. Determination of Sulfide in Brain Tissue by Gas Dialysis/Ion Chromatography: Postmortem Studies and Two Case Reports. *J. Anal. Toxicol.* **1989**, *13* (2), 105−109.

(3) Furne, J.; Saeed, A.; Levitt, M. D. Whole Tissue Hydrogen Sulfide Concentrations Are Orders of Magnitude Lower than Presently Accepted Values. *AJP Regul. Integr. Comp. Physiol.* **2008**, *295* (5), R1479−R1485.

(4) Ishigami, M.; Hiraki, K.; Umemura, K.; Ogasawara, Y.; Ishii, K.; Kimura, H. A Source of Hydrogen Sulfide and a Mechanism of Its Release in the Brain. *Antioxid. Redox Signaling* **2009**, *11* (2), 205−214.

(5) Wintner, E. A.; Deckwerth, T. L.; Langston, W.; Bengtsson, A.; Leviten, D.; Hill, P.; Insko, M. A.; Dumpit, R.; VandenEkart, E.; Toombs, C. F.; Szabo, C. A Monobromobimane-Based Assay to Measure the Pharmacokinetic Profile of Reactive Sulphide Species in Blood: Monobromobimane Assay for Sulphide Detection. *Br. J. Pharmacol.* **2010**, *160* (4), 941−957.

(6) Abe, K.; Kimura, H. The Possible Role of Hydrogen Sulfide as an Endogenous Neuromodulator. *J. Neurosci. Off. J. Soc. Neurosci.* **1996**, *16* (3), 1066−1071.

(7) Hosoki, R.; Matsuki, N.; Kimura, H. The Possible Role of Hydrogen Sulfide as an Endogenous Smooth Muscle Relaxant in Synergy with Nitric Oxide. *Biochem. Biophys. Res. Commun.* **1997**, *237* (3), 527−531.

(8) Moore, P. K., Whiteman, M., Eds. Chemistry, Biochemistry and Pharmacology of Hydrogen Sulfide. In *Handbook of Experimental Pharmacology 230*; Springer International Publishing: Switzerland, 2015.

(9) Zhang, H.; Tang, J.; Liu, X.-P.; Wang, Y.; Yu, W.; Peng, W.-Y.; Fang, F.; Ma, D.-F.; Wei, Z.-J.; Hu, L.-Y. Hydrogen Sulfide Promotes Root Organogenesis in *Ipomoea Batatas, Salix Matsudana* and *Glycine Max*. *J. Integr. Plant Biol.* **2009**, *51* (12), 1086−1094.

(10) Zhang, H.; Hu, L.-Y.; Hu, K.-D.; He, Y.-D.; Wang, S.-H.; Luo, J.-P. Hydrogen Sulfide Promotes Wheat Seed Germination and Alleviates Oxidative Damage against Copper Stress. *J. Integr. Plant Biol.* **2008**, *50* (12), 1518−1529.

(11) Jin, Z.; Pei, Y. Physiological Implications of Hydrogen Sulfide in Plants: Pleasant Exploration behind Its Unpleasant Odour. *Oxid. Med. Cell. Longevity* **2015**, *2015*, 1−6.

(12) Papenbrock, J.; Riemenschneider, A.; Kamp, A.; Schulz-Vogt, H. N.; Schmidt, A. Characterization of Cysteine-Degrading and H_2S-Releasing Enzymes of Higher Plants - From the Field to the Test Tube and Back. *Plant Biol.* **2007**, *9* (5), 582−588.

(13) Ida, T.; Sawa, T.; Ihara, H.; Tsuchiya, Y.; Watanabe, Y.; Kumagai, Y.; Suematsu, M.; Motohashi, H.; Fujii, S.; Matsunaga, T.; Yamamoto, M.; Ono, K.; Devarie-Baez, N. O.; Xian, M.; Fukuto, J. M.; Akaike, T. Reactive Cysteine Persulfides and S-Polythiolation Regulate Oxidative Stress and Redox Signaling. *Proc. Natl. Acad. Sci. U. S. A.* **2014**, *111* (21), 7606−7611.

(14) Kimura, H. Physiological Role of Hydrogen Sulfide and Polysulfide in the Central Nervous System. *Neurochem. Int.* **2013**, *63* (5), 492−497.

(15) Greiner, R.; Pálinkás, Z.; Bäsell, K.; Becher, D.; Antelmann, H.; Nagy, P.; Dick, T. P. Polysulfides Link H_2S to Protein Thiol Oxidation. *Antioxid. Redox Signaling* **2013**, *19* (15), 1749−1765.

(16) Filipovic, M. R. Persulfidation (S-Sulfhydration) and H_2S. In *Chemistry, Biochemistry and Pharmacology of Hydrogen Sulfide*; Moore, P. K., Whiteman, M., Eds.; Springer International Publishing: Cham, Switzerland, 2015; Vol. *230*, pp 29−59.

(17) Ono, K.; Akaike, T.; Sawa, T.; Kumagai, Y.; Wink, D. A.; Tantillo, D. J.; Hobbs, A. J.; Nagy, P.; Xian, M.; Lin, J.; Fukuto, J. M. Redox Chemistry and Chemical Biology of H2S, Hydropersulfides, and Derived Species: Implications of Their Possible Biological Activity and Utility. *Free Radical Biol. Med.* **2014**, *77*, 82−94.

(18) Nishimori, I.; Vullo, D.; Minakuchi, T.; Scozzafava, A.; Osman, S. M.; AlOthman, Z.; Capasso, C.; Supuran, C. T. Anion Inhibition Studies of Two New β-Carbonic Anhydrases from the Bacterial

DOI: 10.1021/acs.jpcb.6b06686
J. Phys. Chem. B XXXX, XXX, XXX−XXX

Pathogen Legionella Pneumophila. *Bioorg. Med. Chem. Lett.* **2014**, *24* (4), 1127−1132.
(19) Kabil, O.; Banerjee, R. Redox Biochemistry of Hydrogen Sulfide. *J. Biol. Chem.* **2010**, *285* (29), 21903−21907.
(20) Kajimura, M.; Fukuda, R.; Bateman, R. M.; Yamamoto, T.; Suematsu, M. Interactions of Multiple Gas-Transducing Systems: Hallmarks and Uncertainties of CO, NO, and H_2S Gas Biology. *Antioxid. Redox Signaling* **2010**, *13* (2), 157−192.
(21) Li, Q.; Lancaster, J. R. Chemical Foundations of Hydrogen Sulfide Biology. *Nitric Oxide* **2013**, *35*, 21−34.
(22) Cooper, C. E.; Brown, G. C. The Inhibition of Mitochondrial Cytochrome Oxidase by the Gases Carbon Monoxide, Nitric Oxide, Hydrogen Cyanide and Hydrogen Sulfide: Chemical Mechanism and Physiological Significance. *J. Bioenerg. Biomembr.* **2008**, *40* (5), 533−539.
(23) Hughes, M. N.; Centelles, M. N.; Moore, K. P. Making and Working with Hydrogen Sulfide. *Free Radical Biol. Med.* **2009**, *47* (10), 1346−1353.
(24) Szabó, C. Hydrogen Sulphide and Its Therapeutic Potential. *Nat. Rev. Drug Discovery* **2007**, *6* (11), 917−935.
(25) Wagner, F.; Asfar, P.; Calzia, E.; Radermacher, P.; Szabó, C. Bench-to-Bedside Review: Hydrogen Sulfide − the Third Gaseous Transmitter: Applications for Critical Care. *Crit. Care* **2009**, *13* (3), 213.
(26) Wever, R.; Van Gelder, B. F.; Dervartanian, D. V. Biochemical and Biophysical Studies on Cytochrome c Oxidase. XX. Reaction with Sulphide. *Biochim. Biophys. Acta, Bioenerg.* **1975**, *387* (2), 189−193.
(27) Collman, J. P.; Ghosh, S.; Dey, A.; Decreau, R. A. Using a Functional Enzyme Model to Understand the Chemistry behind Hydrogen Sulfide Induced Hibernation. *Proc. Natl. Acad. Sci. U. S. A.* **2009**, *106* (52), 22090−22095.
(28) Blackstone, E. H2S Induces a Suspended Animation-Like State in Mice. *Science* **2005**, *308* (5721), 518−518.
(29) Leslie, M. MEDICINE: Nothing Rotten About Hydrogen Sulfide's Medical Promise. *Science* **2008**, *320* (5880), 1155−1157.
(30) Chatfield, M. J.; La Mar, G. N.; Balch, A. L.; Lecomte, J. T. J. Multiple Forms of Sulfmyoglobin as Detected by 1H Nuclear Magnetic Resonance Spectroscopy. *Biochem. Biophys. Res. Commun.* **1986**, *135* (1), 309−315.
(31) Vitvitsky, V.; Yadav, P. K.; Kurthen, A.; Banerjee, R. Sulfide Oxidation by a Noncanonical Pathway in Red Blood Cells Generates Thiosulfate and Polysulfides. *J. Biol. Chem.* **2015**, *290* (13), 8310−8320.
(32) Kraus, D. W.; Wittenberg, J. B. Hemoglobins of the Lucina Pectinata/bacteria Symbiosis. I. Molecular Properties, Kinetics and Equilibria of Reactions with Ligands. *J. Biol. Chem.* **1990**, *265* (27), 16043−16053.
(33) Pietri, R.; Lewis, A.; León, R. G.; Casabona, G.; Kiger, L.; Yeh, S.-R.; Fernandez-Alberti, S.; Marden, M. C.; Cadilla, C. L.; López-Garriga, J. Factors Controlling the Reactivity of Hydrogen Sulfide with Hemeproteins. *Biochemistry* **2009**, *48* (22), 4881−4894.
(34) Bieza, S. A.; Boubeta, F.; Feis, A.; Smulevich, G.; Estrin, D. A.; Boechi, L.; Bari, S. E. Reactivity of Inorganic Sulfide Species toward a Heme Protein Model. *Inorg. Chem.* **2015**, *54* (2), 527−533.
(35) Watanabe, K.; Suzuki, T.; Kitagishi, H.; Kano, K. Reaction between a Haemoglobin Model Compound and Hydrosulphide in Aqueous Solution. *Chem. Commun.* **2015**, *51* (19), 4059−4061.
(36) Nicoletti, F. P.; Comandini, A.; Bonamore, A.; Boechi, L.; Boubeta, F. M.; Feis, A.; Smulevich, G.; Boffi, A. Sulfide Binding Properties of Truncated Hemoglobins. *Biochemistry* **2010**, *49* (10), 2269−2278.
(37) Bakan, A.; Kapralov, A. A.; Bayir, H.; Hu, F.; Kagan, V. E.; Bahar, I. Inhibition of Peroxidase Activity of Cytochrome c: De Novo Compound Discovery and Validation. *Mol. Pharmacol.* **2015**, *88* (3), 421−427.
(38) Vidossich, P.; Alfonso-Prieto, M.; Carpena, X.; Fita, I.; Loewen, P. C.; Rovira, C. The Dynamic Role of Distal Side Residues in Heme Hydroperoxidase Catalysis. Interplay between X-Ray Crystallography and Ab Initio MD Simulations. *Arch. Biochem. Biophys.* **2010**, *500* (1), 37−44.
(39) Fernández-Fueyo, E.; Acebes, S.; Ruiz-Dueñas, F. J.; Martínez, M. J.; Romero, A.; Medrano, F. J.; Guallar, V.; Martínez, A. T. Structural Implications of the C-Terminal Tail in the Catalytic and Stability Properties of Manganese Peroxidases from Ligninolytic Fungi. *Acta Crystallogr., Sect. D: Biol. Crystallogr.* **2014**, *70* (12), 3253−3265.
(40) Ramirez, E.; Cruz, A.; Rodriguez, D.; Uchima, L.; Pietri, R.; Santana, A.; López-Garriga, J.; López, G. E. Effects of Active Site Mutations in Haemoglobin I from *Lucina Pectinata*: A Molecular Dynamic Study. *Mol. Simul.* **2008**, *34* (7), 715−725.
(41) Campomanes, P.; Rothlisberger, U.; Alfonso-Prieto, M.; Rovira, C. The Molecular Mechanism of the Catalase-like Activity in Horseradish Peroxidase. *J. Am. Chem. Soc.* **2015**, *137* (34), 11170−11178.
(42) Fields, J. B.; Hollingsworth, S. A.; Chreifi, G.; Heyden, M.; Arce, A. P.; Magaña-Garcia, H. I.; Poulos, T. L.; Tobias, D. J. Bind and Crawl" Association Mechanism of *Leishmania Major* Peroxidase and Cytochrome *c* Revealed by Brownian and Molecular Dynamics Simulations. *Biochemistry* **2015**, *54* (49), 7272−7282.
(43) Navapour, L.; Mogharrab, N.; Amininasab, M. How Modification of Accessible Lysines to Phenylalanine Modulates the Structural and Functional Properties of Horseradish Peroxidase: A Simulation Study. *PLoS One* **2014**, *9* (10), e109062.
(44) Case, D. A.; Babin, V.; Berryman, J. T.; Betz, R. M.; Cai, Q.; Cerutti, D. S.; Cheatham, T. E., III; Darden, T. A.; Duke, R. E.; Gohlke, H.; et al. *AMBER 14*; University of California: San Francisco, CA, 2014.
(45) Lindorff-Larsen, K.; Piana, S.; Palmo, K.; Maragakis, P.; Klepeis, J. L.; Dror, R. O.; Shaw, D. E. Improved Side-Chain Torsion Potentials for the Amber ff99SB Protein Force Field. *Proteins: Struct., Funct., Genet.* **2010**, *78*, 1950−1958.
(46) *Gaussian 03*; Gaussian, Inc.: Wallingford, CT, 2004.
(47) Soldatova, A. V.; Ibrahim, M.; Olson, J. S.; Czernuszewicz, R. S.; Spiro, T. G. New Light on NO Bonding in Fe(III) Heme Proteins from Resonance Raman Spectroscopy and DFT Modeling. *J. Am. Chem. Soc.* **2010**, *132* (13), 4614−4625.
(48) Marti, M. A.; Crespo, A.; Capece, L.; Boechi, L.; Bikiel, D. E.; Scherlis, D. A.; Estrin, D. A. Dioxygen Affinity in Heme Proteins Investigated by Computer Simulation. *J. Inorg. Biochem.* **2006**, *100* (4), 761−770.
(49) Capece, L.; Marti, M. A.; Crespo, A.; Doctorovich, F.; Estrin, D. A. Heme Protein Oxygen Affinity Regulation Exerted by Proximal Effects. *J. Am. Chem. Soc.* **2006**, *128* (38), 12455−12461.
(50) Marti, M. A.; Capece, L.; Bidon-Chanal, A.; Crespo, A.; Guallar, V.; Luque, F. J.; Estrin, D. A. Nitric Oxide Reactivity with Globins as Investigated Through Computer Simulation. In *Methods in Enzymology*; Elsevier: Amsterdam, 2008; Vol. *437*, pp 477−498.
(51) Scherlis, D. A.; Estrin, D. A. Structure and Spin-State Energetics of an Iron Porphyrin Model: An Assessment of Theoretical Methods. *Int. J. Quantum Chem.* **2002**, *87* (3), 158−166.
(52) Martí, M. A.; Capece, L.; Bikiel, D. E.; Falcone, B.; Estrin, D. A. Oxygen Affinity Controlled by Dynamical Distal Conformations: The Soybean Leghemoglobin and the Paramecium Caudatum Hemoglobin Cases. *Proteins: Struct., Funct., Genet.* **2007**, *68* (2), 480−487.
(53) Perdew, J. P.; Burke, K.; Ernzerhof, M. Generalized Gradient Approximation Made Simple. *Phys. Rev. Lett.* **1996**, *77* (18), 3865−3868.
(54) Nadra, A. D.; Martí, M. A.; Pesce, A.; Bolognesi, M.; Estrin, D. A. Exploring the Molecular Basis of Heme Coordination in Human Neuroglobin. *Proteins: Struct., Funct., Genet.* **2008**, *71* (2), 695−705.
(55) Breneman, C. M.; Wiberg, K. B. Determining Atom-Centered Monopoles from Molecular Electrostatic Potentials. The Need for High Sampling Density in Formamide Conformational Analysis. *J. Comput. Chem.* **1990**, *11* (3), 361−373.
(56) Howes, B. D.; Giordano, D.; Boechi, L.; Russo, R.; Mucciacciaro, S.; Ciaccio, C.; Sinibaldi, F.; Fittipaldi, M.; Martí, M.

DOI: 10.1021/acs.jpcb.6b06686
J. Phys. Chem. B XXXX, XXX, XXX−XXX

A.; Estrin, D. A.; di Prisco, G.; Coletta, M.; Verde, C.; Smulevich, G. The Peculiar Heme Pocket of the 2/2 Hemoglobin of Cold-Adapted Pseudoalteromonas Haloplanktis TAC125. *JBIC, J. Biol. Inorg. Chem.* **2011**, *16* (2), 299−311.
(57) Capece, L.; Lewis-Ballester, A.; Yeh, S.-R.; Estrin, D. A.; Marti, M. A. Complete Reaction Mechanism of Indoleamine 2,3-Dioxygenase as Revealed by QM/MM Simulations. *J. Phys. Chem. B* **2012**, *116* (4), 1401−1413.
(58) Arroyo Mañez, P.; Lu, C.; Boechi, L.; Martí, M. A.; Shepherd, M.; Wilson, J. L.; Poole, R. K.; Luque, F. J.; Yeh, S.-R.; Estrin, D. A. Role of the Distal Hydrogen-Bonding Network in Regulating Oxygen Affinity in the Truncated Hemoglobin III from *Campylobacter Jejuni*. *Biochemistry* **2011**, *50* (19), 3946−3956.
(59) Cohen, J.; Arkhipov, A.; Braun, R.; Schulten, K. Imaging the Migration Pathways for O2, CO, NO, and Xe Inside Myoglobin. *Biophys. J.* **2006**, *91* (5), 1844−1857.
(60) Cohen, J.; Olsen, K. W.; Schulten, K. Finding Gas Migration Pathways in Proteins Using Implicit Ligand Sampling. *Methods in Enzymology*; Elsevier: Amsterdam, 2008; Vol. *437*, pp 439−457.
(61) Forti, F.; Boechi, L.; Bikiel, D.; Martí, M. A.; Nardini, M.; Bolognesi, M.; Viappiani, C.; Estrin, D.; Luque, F. J. Ligand Migration in Methanosarcina Acetivorans Protoglobin: Effects of Ligand Binding and Dimeric Assembly. *J. Phys. Chem. B* **2011**, *115* (46), 13771−13780.
(62) Forti, F.; Boechi, L.; Estrin, D. A.; Marti, M. A. Comparing and Combining Implicit Ligand Sampling with Multiple Steered Molecular Dynamics to Study Ligand Migration Processes in Heme Proteins. *J. Comput. Chem.* **2011**, *32* (10), 2219−2231.
(63) Gabba, M.; Abbruzzetti, S.; Spyrakis, F.; Forti, F.; Bruno, S.; Mozzarelli, A.; Luque, F. J.; Viappiani, C.; Cozzini, P.; Nardini, M.; Germani, F.; Bolognesi, M.; Moens, L.; Dewilde, S. CO Rebinding Kinetics and Molecular Dynamics Simulations Highlight Dynamic Regulation of Internal Cavities in Human Cytoglobin. *PLoS One* **2013**, *8* (1), e49770.
(64) Oliveira, A.; Singh, S.; Bidon-Chanal, A.; Forti, F.; Martí, M. A.; Boechi, L.; Estrin, D. A.; Dikshit, K. L.; Luque, F. J. Role of PheE15 Gate in Ligand Entry and Nitric Oxide Detoxification Function of Mycobacterium Tuberculosis Truncated Hemoglobin N. *PLoS One* **2012**, *7* (11), e49291.
(65) Humphrey, W.; Dalke, A.; Schulten, K. VMD: Visual Molecular Dynamics. *J. Mol. Graphics* **1996**, *14* (1), 33−38.
(66) Isralewitz, B.; Gao, M.; Schulten, K. Steered Molecular Dynamics and Mechanical Functions of Proteins. *Curr. Opin. Struct. Biol.* **2001**, *11* (2), 224−230.
(67) Jensen, M. O.; Park, S.; Tajkhorshid, E.; Schulten, K. Energetics of Glycerol Conduction through Aquaglyceroporin GlpF. *Proc. Natl. Acad. Sci. U. S. A.* **2002**, *99* (10), 6731−6736.
(68) Jarzynski, C. Nonequilibrium Equality for Free Energy Differences. *Phys. Rev. Lett.* **1997**, *78* (14), 2690−2693.
(69) Boechi, L.; Martí, M. A.; Milani, M.; Bolognesi, M.; Luque, F. J.; Estrin, D. A. Structural Determinants of Ligand Migration in Mycobacterium Tuberculosis Truncated Hemoglobin O. *Proteins: Struct., Funct., Genet.* **2008**, *73* (2), 372−379.
(70) Bidon-Chanal, A.; Martí, M. A.; Crespo, A.; Milani, M.; Orozco, M.; Bolognesi, M.; Luque, F. J.; Estrin, D. A. Ligand-Induced Dynamical Regulation of NO Conversion in Mycobacterium Tuberculosis Truncated Hemoglobin-N. *Proteins: Struct., Funct., Genet.* **2006**, *64* (2), 457−464.
(71) Di Lella, S.; Martí, M. A.; Álvarez, R. M. S.; Estrin, D. A.; Ricci, J. C. D. Characterization of the Galectin-1 Carbohydrate Recognition Domain in Terms of Solvent Occupancy. *J. Phys. Chem. B* **2007**, *111* (25), 7360−7366.
(72) Gauto, D. F.; Di Lella, S.; Guardia, C. M. A.; Estrin, D. A.; Martí, M. A. Carbohydrate-Binding Proteins: Dissecting Ligand Structures through Solvent Environment Occupancy. *J. Phys. Chem. B* **2009**, *113* (25), 8717−8724.
(73) Gauto, D. F.; Di Lella, S.; Estrin, D. A.; Monaco, H. L.; Martí, M. A. Structural Basis for Ligand Recognition in a Mushroom Lectin: Solvent Structure as Specificity Predictor. *Carbohydr. Res.* **2011**, *346* (7), 939−948.
(74) López, E. D.; Arcon, J. P.; Gauto, D. F.; Petruk, A. A.; Modenutti, C. P.; Dumas, V. G.; Marti, M. A.; Turjanski, A. G. WATCLUST: A Tool for Improving the Design of Drugs Based on Protein-Water Interactions. *Bioinformatics* **2015**, *31* (22), 3697−3699.
(75) Crespo, A.; Scherlis, D. A.; Martí, M. A.; Ordejón, P.; Roitberg, A. E.; Estrin, D. A. A DFT-Based QM-MM Approach Designed for the Treatment of Large Molecular Systems: Application to Chorismate Mutase. *J. Phys. Chem. B* **2003**, *107* (49), 13728−13736.
(76) Arcon, J. P.; Rosi, P.; Petruk, A. A.; Marti, M. A.; Estrin, D. A. Molecular Mechanism of Myoglobin Autoxidation: Insights from Computer Simulations. *J. Phys. Chem. B* **2015**, *119* (5), 1802−1813.
(77) Choe, Y.-K.; Tsuchida, E.; Ikeshoji, T. First-Principles Molecular Dynamics Study on Aqueous Sulfuric Acid Solutions. *J. Chem. Phys.* **2007**, *126* (15), 154510.
(78) Hu, X. L.; Klimeš, J.; Michaelides, A. Proton Transfer in Adsorbed Water Dimers. *Phys. Chem. Chem. Phys.* **2010**, *12* (16), 3953.
(79) McDonnell, M. T.; Xu, H.; Keffer, D. J. Ab Initio Molecular Dynamics Simulations of an Excess Proton in a Triethylene Glycol-Water Solution: Solvation Structure, Mechanism, and Kinetics. *J. Phys. Chem. B* **2016**, *120* (23), 5223−5242.
(80) Zhang, H.; Ye, Y.-K.; Wang, S.-H.; Luo, J.-P.; Tang, J.; Ma, D.-F. Hydrogen Sulfide Counteracts Chlorophyll Loss in Sweetpotato Seedling Leaves and Alleviates Oxidative Damage against Osmotic Stress. *Plant Growth Regul.* **2009**, *58* (3), 243−250.
(81) Shaik, S.; Kumar, D.; de Visser, S. P.; Altun, A.; Thiel, W. Theoretical Perspective on the Structure and Mechanism of Cytochrome P450 Enzymes. *Chem. Rev.* **2005**, *105* (6), 2279−2328.
(82) Senn, H. M.; Thiel, W. QM/MM Studies of Enzymes. *Curr. Opin. Chem. Biol.* **2007**, *11* (2), 182−187.
(83) Ranaghan, K. E.; Mulholland, A. J. Investigations of Enzyme-Catalysed Reactions with Combined Quantum Mechanics/molecular Mechanics (QM/MM) Methods. *Int. Rev. Phys. Chem.* **2010**, *29* (1), 65−133.
(84) Martí, M. A.; Crespo, A.; Bari, S. E.; Doctorovich, F. A.; Estrin, D. A. QM−MM Study of Nitrite Reduction by Nitrite Reductase of *Pseudomonas Aeruginosa*. *J. Phys. Chem. B* **2004**, *108* (46), 18073−18080.
(85) Martí, M. A.; Capece, L.; Crespo, A.; Doctorovich, F.; Estrin, D. A. Nitric Oxide Interaction with Cytochrome *c* ' and Its Relevance to Guanylate Cyclase. Why Does the Iron Histidine Bond Break? *J. Am. Chem. Soc.* **2005**, *127* (21), 7721−7728.
(86) Crespo, A.; Martí, M. A.; Kalko, S. G.; Morreale, A.; Orozco, M.; Gelpi, J. L.; Luque, F. J.; Estrin, D. A. Theoretical Study of the Truncated Hemoglobin HbN: Exploring the Molecular Basis of the NO Detoxification Mechanism. *J. Am. Chem. Soc.* **2005**, *127* (12), 4433−4444.
(87) Nitsche, M. A.; Ferreria, M.; Mocskos, E. E.; González Lebrero, M. C. GPU Accelerated Implementation of Density Functional Theory for Hybrid QM/MM Simulations. *J. Chem. Theory Comput.* **2014**, *10* (3), 959−967.
(88) González Lebrero, M. C.; Estrin, D. A. QM-MM Investigation of the Reaction of Peroxynitrite with Carbon Dioxide in Water. *J. Chem. Theory Comput.* **2007**, *3* (4), 1405−1411.
(89) Zeida, A.; Babbush, R.; González Lebrero, M. C.; Trujillo, M.; Radi, R.; Estrin, D. A. Molecular Basis of the Mechanism of Thiol Oxidation by Hydrogen Peroxide in Aqueous Solution: Challenging the S_N2 Paradigm. *Chem. Res. Toxicol.* **2012**, *25* (3), 741−746.
(90) Bustamante, J. P.; Abbruzzetti, S.; Marcelli, A.; Gauto, D.; Boechi, L.; Bonamore, A.; Boffi, A.; Bruno, S.; Feis, A.; Foggi, P.; Estrin, D. A.; Viappiani, C. Ligand Uptake Modulation by Internal Water Molecules and Hydrophobic Cavities in Hemoglobins. *J. Phys. Chem. B* **2014**, *118* (5), 1234−1245.
(91) Goldbeck, R. A.; Bhaskaran, S.; Ortega, C.; Mendoza, J. L.; Olson, J. S.; Soman, J.; Kliger, D. S.; Esquerra, R. M. Water and Ligand Entry in Myoglobin: Assessing the Speed and Extent of

DOI: 10.1021/acs.jpcb.6b06686
J. Phys. Chem. B XXXX, XXX, XXX−XXX

Heme Pocket Hydration after CO Photodissociation. *Proc. Natl. Acad. Sci. U. S. A.* **2006**, *103* (5), 1254−1259.
(92) Ouellet, Y. H.; Daigle, R.; Lague, P.; Dantsker, D.; Milani, M.; Bolognesi, M.; Friedman, J. M.; Guertin, M. Ligand Binding to Truncated Hemoglobin N from Mycobacterium Tuberculosis Is Strongly Modulated by the Interplay between the Distal Heme Pocket Residues and Internal Water. *J. Biol. Chem.* **2008**, *283* (40), 27270−27278.
(93) Bustamante, J. P.; Szretter, M. E.; Sued, M.; Martí, M. A.; Estrin, D. A.; Boechi, L. A Quantitative Model for Oxygen Uptake and Release in a Family of Hemeproteins. *Bioinformatics* **2016**, *32*, 1805.
(94) Boechi, L.; Arrar, M.; Marti, M. A.; Olson, J. S.; Roitberg, A. E.; Estrin, D. A. Hydrophobic Effect Drives Oxygen Uptake in Myoglobin via Histidine E7. *J. Biol. Chem.* **2013**, *288* (9), 6754−6762.
(95) Scott, E. E.; Gibson, Q. H.; Olson, J. S. Mapping the Pathways for O2 Entry Into and Exit from Myoglobin. *J. Biol. Chem.* **2001**, *276* (7), 5177−5188.
(96) Boechi, L.; Mañez, P. A.; Luque, F. J.; Marti, M. A.; Estrin, D. A. Unraveling the Molecular Basis for Ligand Binding in Truncated Hemoglobins: The trHbO Bacillus Subtilis Case. *Proteins: Struct., Funct., Genet.* **2010**, *78* (4), 962−970.
(97) Capece, L.; Boechi, L.; Perissinotti, L. L.; Arroyo-Mañez, P.; Bikiel, D. E.; Smulevich, G.; Marti, M. A.; Estrin, D. A. Small Ligand−globin Interactions: Reviewing Lessons Derived from Computer Simulation. *Biochim. Biophys. Acta, Proteins Proteomics* **2013**, *1834* (9), 1722−1738.
(98) Liphardt, J. Equilibrium Information from Nonequilibrium Measurements in an Experimental Test of Jarzynski's Equality. *Science* **2002**, *296* (5574), 1832−1835.
(99) Marques, H. M.; Perry, C. B. Hemepeptide Models for Hemoproteins: The Behavior of N-Acetylmicroperoxidase-11 in Aqueous Solution. *J. Inorg. Biochem.* **1999**, *75* (4), 281−291.
(100) Brunori, M.; Amiconi, G.; Antonini, E.; Wyman, J.; Zito, R.; Rossi Fanelli, A. The Transition between "acid" and "alkaline" Ferric Heme Proteins. *Biochim. Biophys. Acta, Protein Struct.* **1968**, *154* (2), 315−322.
(101) Sun, J.; Wilks, A.; Ortiz de Montellano, P. R.; Loehr, T. M. Resonance Raman and EPR Spectroscopic Studies on Heme-Heme Oxygenase Complexes. *Biochemistry* **1993**, *32* (51), 14151−14157.
(102) Takahashi, S.; Wang, J.; Rousseau, D. L.; Ishikawa, K.; Yoshida, T.; Host, J. R.; Ikeda-Saito, M. Heme-Heme Oxygenase Complex. Structure of the Catalytic Site and Its Implication for Oxygen Activation. *J. Biol. Chem.* **1994**, *269* (2), 1010−1014.
(103) Song, Y.; Michonova-Alexova, E.; Gunner, M. R. Calculated Proton Uptake on Anaerobic Reduction of Cytochrome C Oxidase: Is the Reaction Electroneutral? *Biochemistry* **2006**, *45* (26), 7959−7975.

DOI: 10.1021/acs.jpcb.6b06686
J. Phys. Chem. B XXXX, XXX, XXX−XXX